Flutter Prediction for Aircraft Conceptual Design

Wu Li,* Karl Geiselhart,† and Jay Robinson†
NASA Langley Research Center, Hampton, Virginia 23681, USA

Flutter prediction is usually a knowledge-based analysis process that aims to reduce the cost of aeroelastic stability margin certification. However, early detection of flutter problems is beneficial in the development of unconventional aircraft. The recently developed automation tool ConceptFEA for structural sizing of aircraft concepts paves the way for rapid physics-based flutter prediction of aircraft concepts. A match-point iteration procedure using the p-k method is implemented for ConceptFEA with minimum user input requirements to generate flutter boundary points. A subsonic business jet concept and its high aspect-ratio wing variant are used to demonstrate how the newly developed flutter prediction capability can be used during aircraft conceptual design. Sized structures, flutter boundary curves, and flutter sensitivity analysis results are generated for these two concepts using ConceptFEA. The relevant equivalent plate theory is provided to show the quantitative relationships between a stiffened panel and its equivalent NASTRAN PSHELL panel. The rapid flutter prediction capability of ConceptFEA makes multidisciplinary collaborations between systems analysts and aeroelasticity experts feasible in practice.

Nomenclature

A_{11}	=	maximum membrane stiffness of stiffened or unstiffened panel
A_S	=	cross section area of uniaxial stiffener
b_l, b_u	=	lower and upper bounds for flutter air density in the match-point iteration procedure
c	=	speed of sound
D_{11}	=	maximum bending stiffness of stiffened or unstiffened panel with respect to neutral axis
D_{11}^*	=	scaled bending stiffness of equivalent panel defined by NASTRAN PSHELL
D_{yy}	=	maximum bending stiffness of stiffened panel with respect to neutral axis
g, g_s	=	damping coefficient
f_1, f_N	=	frequency in Hz
h(web)	=	thickness of web of stiffener
h_S	=	thickness of equivalent-stiffener layer
h_S(skin)	=	thickness of base plate of stiffened plate
H(stiffener)	=	height of stiffener
i	=	imaginary unit $\sqrt{-1}$
Im(p)	=	imaginary part of p
j, s	=	integer index
$\mathbf{K}$	=	generalized stiffness matrix
k, k_1, k_j	=	reduced frequency
k_{min}, k_{max}	=	lower and upper bounds for reduced frequency range in the match-point iteration procedure
L	=	reference length in flutter equation
$\mathbf{M}$	=	generalized mass matrix
M	=	constant Mach number in flutter equation
M_D	=	dive Mach number
M_f	=	predicted flutter Mach number
M_{min}, M_{max}	=	lower and upper bounds for Mach speed range in the match-point iteration procedure
M_V	=	Mach number corresponding to velocity V
MTOW	=	maximum take-off weight

* Senior Research Engineer, Aeronautics Systems Analysis Branch
† Aerospace Engineer, Aeronautics Systems Analysis Branch

n, n_1, n_2 = positive integer
N = number of flexible vibration modes for flutter analysis
p, p_s = complex eigenvalue of flutter equation
$\mathbf{q}$ = eigenvector of flutter equation
$\mathbf{Q^I}$ = imaginary part of generalized aerodynamic force matrix
$\mathbf{Q^R}$ = real part of generalized aerodynamic force matrix
R = region consisting of cross sections of a stiffener and a segment of base plate
V, V_s = velocity
V_D = dive velocity
V_f = flutter velocity
$V_{\min}, V_{\max}$ = minimum and maximum velocities for flutter analysis using p-k method, respectively
y, z = coordinates of a point on a plane
Z, Z_0 = altitude
ZFW = zero fuel weight
β = scaling parameter for bending stiffness of NASTRAN PSHELL element
$\delta, \delta_1, \delta_2$ = positive number
ρ, ρ_1, ρ_2 = air density
ρ_{next} = predicted air density corresponding to flutter Mach
ω, ω_s = imaginary part of p, p_s

I. Introduction

THE p-k method [1-3] is an acceptable flutter prediction method for the Federal Aviation Administration (FAA) aeroelastic stability margin certification of new aircraft. The challenge is to build a structural model that exhibits the same vibration modes as the complete aircraft. Ground vibration tests are usually conducted to calibrate the structural model. Therefore, any validated flutter prediction is usually available at the late stage of new aircraft development.

Flutter analysis of a complete aircraft as a scientific research discipline is very costly, partially due to the difficulty in validating the FEM required for flutter analysis and the volume of the information required to document it. Ascertaining all the key information for the reported flutter boundary computation is difficult in the open literature. The most detailed example is the match-point flutter analysis of a complete F-16 aircraft configuration in the ZONA Application Manual Vol. 1 [4], where the input file for the match-point flutter solution is provided. This example shows the match-point flutter analysis at a constant Mach number of 0.9 with varying altitude using ZONA's g-method. In general, the flutter boundary of a configuration is represented by a few data points in a (Mach, Altitude) or (Mach, Dynamic Pressure) plot [5-10].

The motivation for enhancing the automated structural sizing tool ConceptFEA [11] with a flutter prediction capability is to enable flutter assessment and mitigation during the early conceptual design phase, a much needed analysis capability for the development of unconventional aircraft. Initially, ConceptFEA was developed for structural sizing of panel thicknesses of an aircraft concept using a finite-element model (FEM) of quadrilaterals and some triangles. ConceptFEA integrates weight and mission data from the Flight Optimization System (FLOPS) [12] in finite-element analysis (FEA); it only requires a parametric definition of a 2D layout of spars, ribs, and frames/bulkheads for automated generation of a FEM mesh for wing and fuselage of any OpenVSP [13] geometry. Aero panels for aerodynamic surfaces (such as wing, canard, aileron, and tails) are also automatically generated using two input parameters that define the desired panel size and the minimum number of aero panels in the flow direction. Aero-structural coupling is defined via NASTRAN [14] SPLINE1 and the load bearing nodes are mapped to the corresponding aero panels with a proximity projection algorithm. All tedious manual steps for allocation of fuel tanks, fuel distribution, attachments for point weights, definitions of trim conditions, and assignments of material properties are automated and can be completed in minutes. The PATRAN [15] Paver is used to generate FEM meshes of the FEM-ready geometry model [16] constructed by ConceptFEA. A post-meshing algorithm of ConceptFEA ensures no disconnection between two adjacent panels in the generated FEM mesh for wing and fuselage. For any OpenVSP aircraft configuration with a wing and fuselage, a mathematically correct model for sizing of wing and fuselage structural panels can be generated in less than one day. In this paper, ConceptFEA is extended for flutter boundary prediction of the sized FEM model of an aircraft concept.

For ease of use, an iterative process based on the NASTRAN p-k method is implemented to compute a match-point flutter solution for any constant Mach number and the required inputs for the NASTRAN p-k method are also reduced to a minimum. To obtain a match-point flutter solution, a user only needs to provide a target flutter Mach

number, a Mach range, the number of modes for flutter analysis, an initial guess for the flutter altitude, and an error tolerance for the computed flutter Mach number.

A configuration similar to the Gulfstream G450 (G450-like) and its high aspect-ratio (AR) wing variant (G450-AR24) are used to demonstrate the feasibility of the developed flutter analysis capability for aircraft conceptual design. Finite-element models of both configurations are generated/sized using ConceptFEA and flutter studies are conducted with the sized configurations. The flutter analysis results include flutter boundary prediction and sensitivity of flutter altitude with respect to a variety of modeling parameters, such as structural and aero panel resolutions, the number of modes for flutter analysis, bending stiffness scaling parameter, and wing sweep angle.

The paper is organized as follows. Section II introduces the match-point iteration procedure using the NASTRAN p-k method for finding a match-point flutter solution. Conceptual design, structural sizing, and flutter analysis of G450-like and G450-AR24 are given in Section III. Subsection III.A documents the conceptual design and structural sizing of the two aircraft concepts. Subsection III.B contains the flutter boundary curves of the two concepts for Mach numbers from 0.4 to 1.2. Subsection III.C provides the flutter sensitivity results with respect to numerical solution parameters (such as structural and aero panel resolutions) and system-level design parameters (such as wing sweep angle) for G450-AR24. Concluding remarks are included in Section IV. Appendices I-III are the technical details of numerical algorithms used in the match-point iteration procedure. Appendix IV reviews the basic theory on the relationships between a stiffened plate and its equivalences. This appendix lays the theoretical foundation to extract meaningful information of as-built panels from a sized structure model of equivalent panels. Moreover, the theory also helps conceptual designers to set up parameters of equivalent panels using information of as-built panels of existing aircraft.

II. Match-Point Flutter Solution

In theory, once an aeroelastic analysis model for NASTRAN is generated, it is relatively easy to manually modify the case control parameters for a flutter analysis. In practice, it takes experience to set up the required reduced frequency range and velocity range for a flutter analysis using the NASTRAN p-k method [3]. Finding a mathematically correct [or match-point] flutter solution might require multiple runs of the NASTRAN p-k method and manual post-processing of NASTRAN outputs. The goal of this section is to document the automation procedure used by ConceptFEA that simplifies the key inputs for a match-point flutter solution to the following conceptual-level inputs: a constant [flutter] Mach number M and a Mach range containing M. The outputs of the automated match-point flutter solution procedure include the calculated flutter Mach M_f and flutter altitude.

For a specific operating condition (such as flying with full or zero fuel weight), the flutter boundary consists of Mach and altitude pairs (M, Z) such that M is the flutter Mach of the configuration at altitude Z. Each boundary point requires a match-point flutter solution of the flutter equation. The flutter equation for the p-k method can be written as follows [1-3]:

$$\left[\left(\frac{V^2}{L^2}\right)\cdot\mathbf{M}\cdot p^2+\mathbf{K}-\frac{1}{2}\cdot\rho\cdot V^2\cdot\left(\mathbf{Q^R}(M,k)+\frac{p}{k}\mathbf{Q^I}(M,k)\right)\right]\cdot\{\mathbf{q}\}=0 \tag{1}$$

Here $\mathbf{M}$ and $\mathbf{K}$ are the generalized mass and stiffness matrices, respectively; $\mathbf{Q^R}$ and $\mathbf{Q^I}$ are the real and imaginary parts of the generalized aerodynamic force matrix that depends on Mach number M and reduced frequency k. Parameter V is the velocity of undisturbed flow, L is the reference length, ρ is the air density, and $p = g + i\cdot\omega$ is a non-dimensional Laplace [complex] parameter and is also referred to as an eigenvalue of Eq. (1). The imaginary part of p must satisfy the following consistency condition:

$$k=\left(\frac{L}{V}\right)\cdot\mathrm{Im}(p),\ i.e.,\ \ k=\left(\frac{L}{V}\right)\cdot\omega \tag{2}$$

The NASTRAN p-k method requires users to specify L, ρ, and M for flutter analysis. The reference length L is usually a half of the average chord length of the wing. If known in advance, ρ should be the air density of the flight altitude where flutter occurs and M should be the Mach number corresponding to the flutter speed at the flight altitude.

For numerical analysis requirements, the NASTRAN p-k method needs an error tolerance for solving Eq. (2) iteratively, a sequence of reduced frequencies $\{k_j\}$ for calculating the generalized aerodynamic force matrices $\mathbf{Q^R}$ and $\mathbf{Q^I}$, and a sequence of velocities $V_1 < V_2 < \cdots < V_n$ around the flutter velocity. The matrices $\mathbf{Q^R}(M,k)$ and $\mathbf{Q^I}(M,k)$ for an arbitrary k are computed using numerical interpolations of $\{\mathbf{Q^R}(M, k_j)\}$ and $\{\mathbf{Q^I}(M, k_j)\}$, respectively. For each vibration mode included in flutter analysis, the NASTRAN p-k method outputs a sequence of eigenvalues $p_s = g_s + i\cdot\omega_s$ corresponding to velocities V_s ($s = 1,\ldots,n$). The curve representing $\{(V_s, g_s)\}$ is called the damping curve for the

vibration mode and any intersection point of the damping curve and $g = 0$ defines a possible flutter velocity V_f, which is the V-coordinate of the intersection point. In this paper, velocities V_s are replaced by their corresponding Mach numbers M_{Vs} with respect to the air density ρ. For example, Fig. 1 shows the damping curves with respect to Mach number M_V (converted from V) for four vibration modes used in flutter analysis. Possible flutter Mach numbers are identified for mode 1 and mode 4, but the predicted flutter Mach M_f is 1.2. When multiple intersection points exist, only the lowest Mach coordinate of the intersection points can be used as M_f. In general, for a constant M, the configuration only flutters at an air density lower than ρ if $M_f < M$; while the configuration only flutters at an air density higher than ρ if $M_f > M$. One can adjust ρ so that $M_f = M$, then the corresponding flutter solution is called a match-point flutter solution. The name comes from the fact that the predicted flutter Mach number M_f matches the Mach number M that defines the flutter Eq. (1).

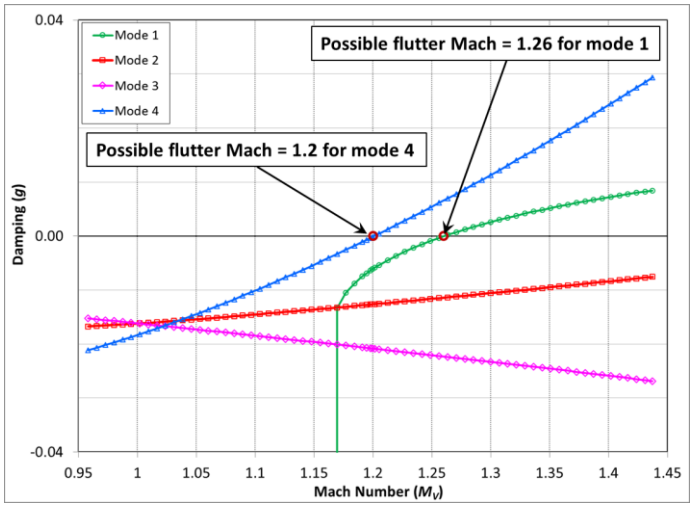

Fig. 1 Identification of flutter points using damping curves.

In summary, for the NASTRAN p-k method, a match-point flutter solution must yield M_f with the following properties: (i) $(M_f, 0)$ is an intersection point of a damping curve and $g = 0$, (ii) the damping curve must change sign from negative to positive when crossing the intersection point, (iii) M_f is the smallest among all Mach numbers with the previous two properties, and (iv) $M_f = M$. For a match-point flutter solution, the corresponding air density ρ is called the flutter air density and the vibration mode corresponding to the damping curve that defines M_f is called the flutter mode. The altitude corresponding to the flutter air density is called the flutter altitude.

Note that ρ and M are given before flutter analysis begins, it is unlikely that the flutter solution for Eq. (1) is a match-point flutter solution. For a constant Mach number M, one could adjust ρ iteratively to find a match-point flutter solution of Eq. (1). In the remaining part of this section, an iterative procedure using the NASTRAN p-k method is introduced to find the air density ρ such that $M_f = M$. Moreover, the required inputs for the NASTRAN p-k method are reduced to a constant [flutter] Mach number M, a Mach range containing M, the number of points for damping curves, the number of vibration modes for flutter analysis, and an initial guess for flutter altitude. These inputs don't require any in-depth knowledge about flutter analysis.

Match-Point Iteration Procedure. Assume that $0 < M_{\min} < M < M_{\max}$ such that $M \neq 1$, n is the number of points for damping curves, $N > 0$ is the number of vibration modes for flutter analysis, Z_0 is an initial guess for the flutter altitude (which could be negative). Then a match-point flutter solution for M can be obtained by the following iteration procedure.

1. Run a modal analysis for N flexible modes.
2. Extract the natural frequencies f_1 and f_N (in Hz) of the first and Nth flexible modes.
3. Calculate the air density ρ at altitude Z_0.
4. Let c be the speed of sound for density ρ.
5. Let $V_{\min} = c \cdot M_{\min}$, $V_{\max} = c \cdot M_{\max}$, and $V_f = c \cdot M$.
6. Find exactly n velocities $\{V_s: 1 \le s \le n\}$ (including V_f) as evenly distributed in the interval $[V_{\min}, V_{\max}]$ as possible but with some clustering around V_f using the method in Appendix I.
7. Let $k_{\min} = 2 \cdot \pi f_1 \cdot L/V_{\max}$ and $k_{\max} = 2 \cdot \pi f_N \cdot L/V_{\min}$.

8. Find a sequence of reduced frequencies $\{k_j\}$ from 0.001 to k_{max} using the method in Appendix II.
9. Use the NASTRAN p-k method to find a flutter solution for the specified inputs L, M, N, ρ, $\{k_j\}$, and $\{V_s\}$.
10. Find the predicted flutter Mach M_f using the damping curves.
11. If $|M_f - M| < 0.001 \cdot M$ is not true, use Eq. (3) to define ρ_{next} if feasible, reset $\rho = \rho_{next}$, and go back to Step 4. Details for exceptional cases in this step are described in Appendix III.

$$\rho_{\text{next}} = \left(\frac{M_f}{M}\right)^2 \cdot \rho \tag{3}$$

12. Output M_f as the match-point flutter Mach, ρ as the flutter air density, and the altitude Z corresponding to ρ as the flutter altitude.

The relative error tolerance of 0.001 for matching the Mach numbers in Step 11 can be replaced by any other desired tolerance. In general, if the interval $[M_{min}, M_{max}]$ is larger, then the iteration procedure is more efficient to find a match-point flutter solution (cf. Appendix III). But a larger $[M_{min}, M_{max}]$ tends to reduce the damping curve resolution, which determines the numerical accuracy of using interpolation to compute M_f. The damping curve resolution is also controlled by n. Increasing n incurs more computational time. For the numerical results generated in this paper, $M_{min} = 0.9 \cdot M$, $M_{max} = 1.1 \cdot M$, $n = 60$, and N is the largest integer such that the first N flexible modes don't contain any local vibration mode. In practice, the value of N is determined by visual inspection of vibration modes after the modal analysis for a sufficiently large number of modes.

In general, M_f is actually a decreasing function of ρ., i.e.,

$$M_f(\rho_1) < M_f(\rho_2) \text{ if } \rho_1 > \rho_2 \tag{4}$$

If Eq. (4) holds true for a constant Mach number M, then the above iteration procedure is guaranteed to find a match-point flutter solution for M.

III. Flutter Prediction for Conceptual Design

For aeroelastic stability margin, the FAA regulations require that "*the airplane must be designed to be free from aeroelastic instability for all configurations and design conditions within the aeroelastic stability envelopes, which include all combinations of altitudes and speeds encompassed by the V_D / M_D versus altitude envelope enlarged at all points by an increase of 15 percent in equivalent airspeed at both constant Mach number and constant altitude*" (cf. FAR 25-629 (b)(1) [17]). It is feasible to verify aeroelastic stability in the aeroelastic stability envelope for a sized configuration with full fuel or zero fuel using ConceptFEA during conceptual design.

Two aircraft concepts are used to demonstrate the complete aeroelastic stability analysis process starting from an OpenVSP model representing an aircraft concept to the final assessment of the flutter characteristics of the aircraft. The first concept, G450-like, is similar to the Gulfstream G450 business jet; and the second one, G450-AR24, replaces the wing of G450-like with a wing of aspect ratio 24. Subsection III.A documents the conceptual design and structural sizing of these two concepts. Results of match-point flutter solutions for Mach number from 0.4 to 1.2 are included in Subsection III.B. For these two concepts, a cruise Mach of 0.85 implies $M_D = 0.98$ and the FAA aeroelastic stability envelope extends to Mach = $1.15 \cdot M_D = 1.124$. Therefore, sensitivity analyses of flutter altitude for G450-AR24 near the maximum Mach in the aeroelastic stability envelope are also performed in Subsection III.C. The sensitivity is about the flutter altitude variation with respect to changes of structural and aero panel resolutions, the number of modes for flutter analysis, and bending stiffness scaling parameter. Moreover, the sensitivity results in Subsection III.C also show how the flutter characteristics of G450-AR24 are affected by wing sweep angle.

A. G450 and Its High Aspect-Ratio Variant

Based on the Gulfstream G450 specification sheets [18], the G450-like concept is generated using OpenVSP (cf. Fig. 2(a)). Its FLOPS sizing is performed for a cruise Mach of 0.85, a design range of 3,000 nmi, and maximum payload of 6,095 lb (vs 6,000 lb for the actual G450). The resulting maximum take-off weight (MTOW) of G450-like is 74,600 lb (vs 74,600 lb for the actual G450), and zero fuel weight (ZFW) of G450-like is 48,150 lb (vs 49,000 lb for the actual G450). FLOPS weight estimates for the as-built wing and fuselage are 5,727 lb and 5,885 lb, respectively. The structural layout of G450-like follows a cutaway drawing of a Gulfstream G450. The sizing constraints are defined by a safety factor of 1.7 for stress tolerance under 2.5G, 1G, and -1G pitch maneuvers at cruise Mach of 0.85 with the start cruise weight of 72,339 lb. The minimum gauges for wing and fuselage equivalent panels

are 0.12 in and 0.15 in, respectively. Non-structural portions of wing and fuselage weights are automatically determined based on FLOPS empirical formulas (cf. Ref. [11]). The only exception is that the total non-structural mass of the wing is increased by 300 lb for a better match between the ConceptFEA and FLOPS wing weights. A mesh of 14,191 quadrilaterals and some triangles (cf. Fig. 2(b)) is used for finite-element analysis. For aerodynamics, 791 aero panels are used for the wing and horizontal tail. A generic aluminum material (2024-T3), with yield stress of 47,000 psi, is used for all panels. The sized solution generated by ConceptFEA has a total wing weight of 5,571 lb and a total fuselage weight of 5,885 lb, which differ from FLOPS wing and fuselage weights by less than 2.7% and 0.1%, respectively.

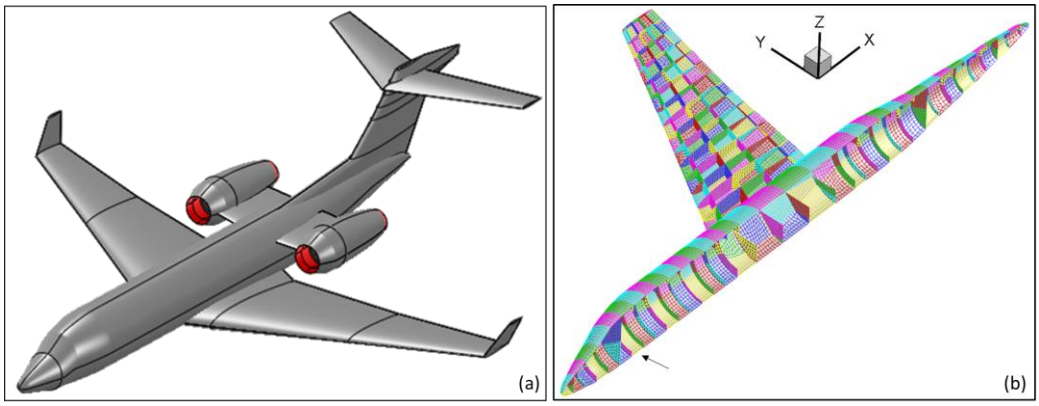

Fig. 2 (a) OpenVSP geometry and (b) finite-element mesh of G450-like.

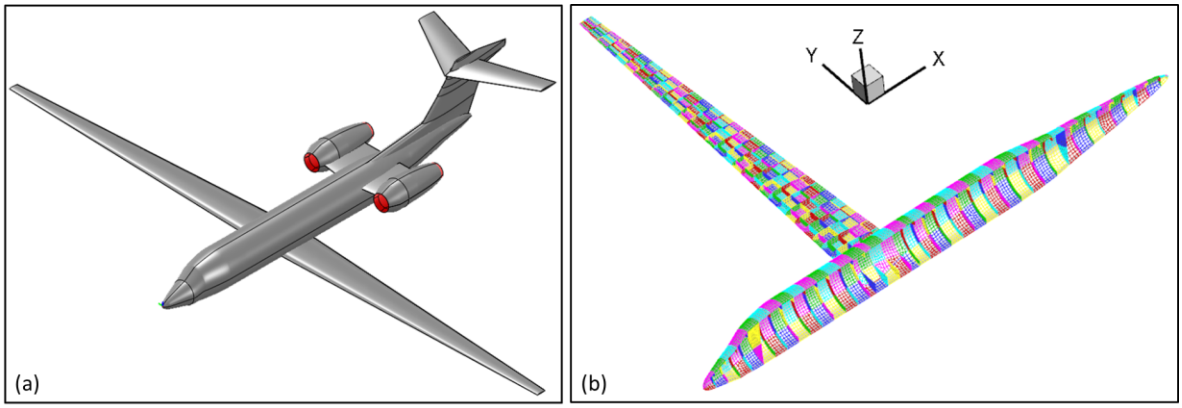

Fig. 3 (a) OpenVSP geometry and (b) finite-element mesh of G450-AR24.

To generate a high aspect-ratio wing variant of G450-like, the wing planform is changed to a trapezoidal shape with wing sweep angle of 0.5°. The reason for selecting a sweep angle of 0.5° is to use a minimum sweep angle that can still cruise at Mach number of 0.85 without excessive loss of performance. Such a wing planform is more likely to flutter as discovered during a concept exploration process and a fluttering concept helps to verify whether ConceptFEA can capture the flutter physics correctly. The resulting wing planform is completely determined after setting the tip airfoil chord length to 2 ft and wing aspect ratio to 24, which leads to a reasonable wing planform for G450-AR24 shown in Fig. 3(a). The increased lift-to-drag ratio of the high aspect-ratio wing saves 10% of the fuel for the same mission compared to the G450-like wing. This is mainly due to a significant increase of wing weight of G450-AR24 and the high cruise Mach for an unswept wing. For easy comparison, some of the conceptual design information of G450-like and G450-AR24 are listed in Table 1.

Table 1 Comparison of G450-like and G450-AR24.

Concept	MTOW	ZFW	Fuel	Wing Weight	Wing Area	Wing Span	Aspect Ratio	Lift/Drag
G450-like	74,600 lb	48,151 lb	22,436 lb	5,727 lb	893.6 ft^2	70 ft	5.8	16.4
G450-AR24	93,845 lb	69,539 lb	20,148 lb	26,922 lb	700.0 ft^2	130 ft	24	25.0

The structural layout of G450-AR24 is similar to G450-like (cf. Figs. 2(b) and 3(b)), except that the rib spacing is about 2 ft based on empirical data for rib spacing reported in Ref. [19]. The FLOPS sizing is performed for G450-AR24 using the same speed, range, and payload requirements as G450-like. The structural sizing constraints of G450-AR24 are identical to those of G450-like except for two modifications. To make the sized G450-AR24 easier to flutter, the safety factor for stress tolerance is reduced from 1.7 to the minimum FAA requirement of 1.5. Another modification is related to the non-structural component of the FLOPS wing weight. The FLOPS wing weight for G450-like is 5,727 lb, and its non-structural component is 894 lb. In contrast, the FLOPS wing weight for G450-AR24 is 26,922 lb, and its non-structural component is 648 lb. Because the FLOPS non-structural component of wing weight is a function of wing area based on the existing aircraft weight data and G450-AR24 is totally outside of the database used to develop FLOPS weight equations, some redistribution of the FLOPS wing weight between structural and non-structural components for G450-AR24 is required. An additional 10,000 lb of the structural portion of the FLOPS wing weight is bookkept as non-structural weight that must be carried by the wing structural panels during the structural sizing.

A structural mesh of 13,003 quadrilaterals and some triangles (cf. Fig. 3(b)) is used for finite-element analysis. Figure 4(a) shows 2,083 wing aero panels along with tail aero panels for aerodynamic analysis and Fig. 4(b) shows the attached fuel and FLOPS weights for the structural sizing model. ConceptFEA finds an optimal sizing solution that has maximum displacements of 11.8 ft, 4.7 ft, and 4.7 ft for 2.5G, 1G, and -1G pitch maneuvers, respectively.

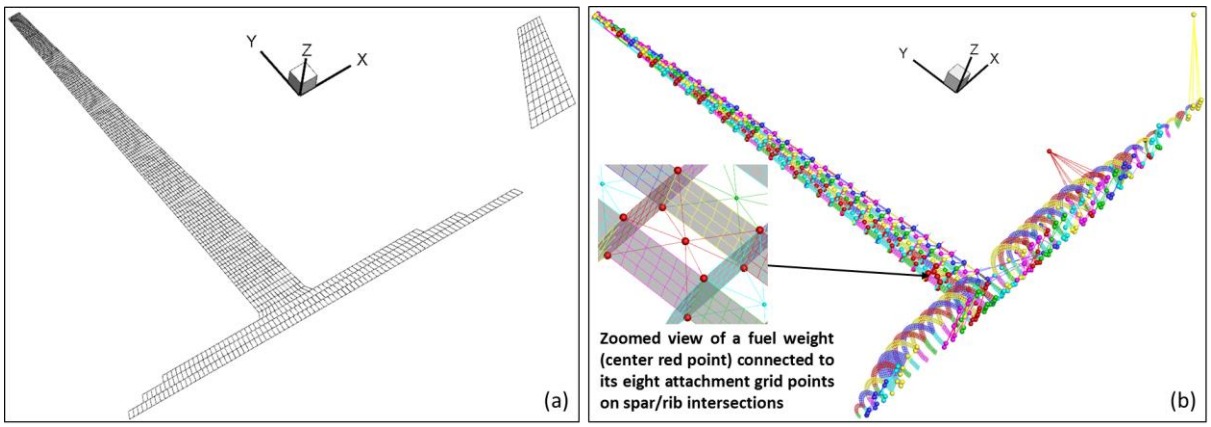

Fig. 4 (a) Aero panels and (b) attached point weights for structural sizing model of G450-AR24.

The sized structure of G450-AR24 has a total wing weight of 19,120 lb and a total fuselage weight of 6,533 lb. Note that ConceptFEA's conservative estimate of wing weight for G450-AR24 (assuming 40% of the as-built wing weight from FLOPS is non-structural weight) is still much lower than the detailed wing weight estimate of 26,922 lb from FLOPS. The simple wing weight estimate of FLOPS for G450-AR24 is 13,798 lb, which is about a half of the detailed wing weight. In contrast, the simple wing weight estimate of FLOPS for G450-like is 5,565 lb, which differs from the detailed wing weight of 5,727 lb by less than 4%. The wing weight of G450-AR24 generated by ConceptFEA is between the simple and detailed wing weight estimates from FLOPS. A reliable weight estimate for G450-AR24 requires further research, but it is beyond the scope of this paper. The advantage of the ConceptFEA wing weight estimate is that all the assumptions used to derive the wing weight of 19,120 lb are explicitly stated for a FEM-based structural sizing model and a conceptual designer could determine whether more operating conditions, design constraints, or analysis fidelity should be used for a more reliable wing weight estimate.

B. Flutter Boundary Prediction

After structural sizing, a modal analysis is performed to see which modes are global vibration modes suitable for flutter analysis. A finite-element model using equivalent panels tends to have unrealistic local vibration modes that don't exist in a detailed structure model using stiffened panels. Mathematically, one could artificially increase the bending stiffness scaling parameter β of PSHELL elements in NASTRAN to eliminate the local vibration modes. Practically, β is not a free design variable and depends on how stiffened panels are constructed (cf. Appendix IV). For all the flutter analysis results in this paper, β = 100 unless stated otherwise.

For each concept, the number of modes, *N*, for flutter analysis is the largest integer such that the first *N* flexible modes are global vibration modes. Figure 5 shows the 14th and 15th flexible mode shapes for ZFW of G450-AR24. Because the 15th flexible mode is obviously a local vibration mode and the first 14 flexible modes are global modes

(by visual inspection), $N = 14$ is chosen for flutter analysis of G450-AR24 to exclude unrealistic local vibration modes. Similarly, $N = 6$ is selected for flutter analysis of G450-like.

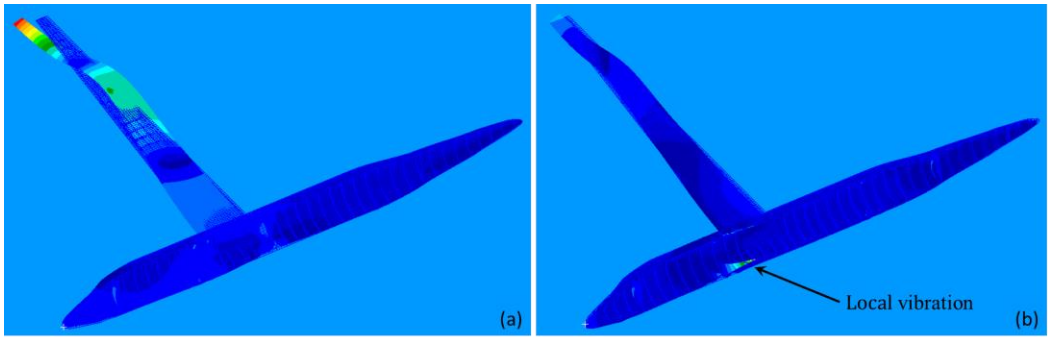

Fig. 5 (a) The 14th and (b) 15th flexible mode shapes for ZFW of G450-AR24 when $\beta = 100$.

The G450 flight envelope in Fig. 6 is based on an online G450 Mach flight envelope figure [20]. All points but one on the flutter margin (i.e., aeroelastic stability margin) are generated by multiplying the Mach numbers corresponding to points on the right-hand side of the G450 flight envelope by 1.15^2, based on the FAA rules for dive Mach and flutter margin. The point on the flutter margin at altitude of about -10,000 ft is based on the margin requirement for dive Mach at sea level. In reality, many configurations and operating conditions have to be verified for the flutter margin requirement; however, for simplicity, only ZFW and MTOW for level flight are analyzed in this paper. Fourteen Mach numbers from 0.4 to 1.2 are selected to generate the flutter boundary curves. For each selected M, $M_{min} = 0.9 \cdot M$ and $M_{max} = 1.1 \cdot M$. The damping curve resolution parameter n is 60 and the initial guess Z_0 for flutter altitude corresponding to $M = 0.4$ is -90,000 ft. After generating the flutter boundary point for $M = 0.4$, the computed flutter altitude with respect to the previous Mach number is used as Z_0 by the match-point iteration procedure for a new Mach number. Figure 6 shows the calculated flutter boundary curves for G450-like and G450-AR24 configurations with zero and full fuel weights. The average wall time for a match-point flutter solution is about 3 mins for G450-like and 10 mins for G450-AR24 using a desktop computer with 32GB RAM and 3.6GHz Intel Xeon CPU (E5-1650 v4).

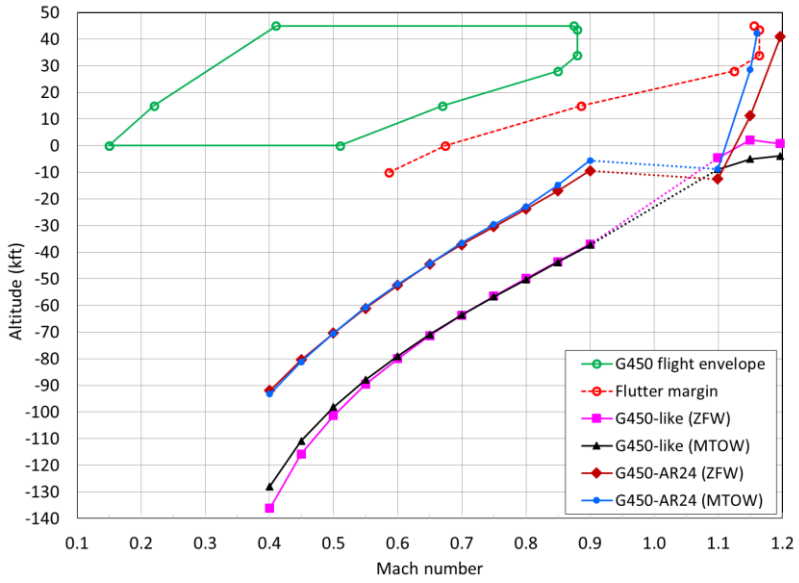

Fig. 6 Flutter boundary curves for G450-like and G450-AR24.

A configuration satisfies the flutter margin requirement if its flutter boundary curve does not intersect the region on the left-hand side of the flutter margin curve. Based on Fig. 6, ZFW and MTOW of G450-like satisfy the flutter margin requirement, while MTOW of G450-AR24 violates the flutter margin requirement and the flutter boundary curve for ZFW of G450-AR24 is perhaps too close to the flutter margin curve.

For MTOW of G450-AR24, the flutter boundary curve has a point at $M = 1.16$ instead of 1.2. This is due to failure of the match-point iteration procedure in search of a match-point flutter solution for $M = 1.2$. In this failed case, during the iterations, when a computed flutter Mach is less than 1.2, the air density ρ becomes an upper bound b_u for the flutter air density. After a few iterations, predicted flutter Mach does not exist when ρ is low enough. This sets ρ as a lower bound b_l for the flutter air density. Afterward, the match-point iteration procedure attempts to find the flutter air density in the interval $[b_l, b_u]$ and the search fails when there is no match-point flutter solution for any ρ between b_l and b_u.

Manual selections of M between 1.15 and 1.2 are used to define the flutter boundary curve for MTOW of G450-AR24 between 1.15 and 1.2. The match-point iteration procedure finds the flutter altitude of 42,200 ft for $M = 1.16$. It appears that the wing twist flutter mode for MTOW of G450-AR24 is suppressed by the aero forces and does not flutter anymore when M is between 1.17 and 1.2. Further study is needed to fully understand why a configuration would have no match-point flutter solution for a particular Mach number.

C. Sensitivity Analysis of Flutter Altitude

Sensitivity analysis is performed for ZFW of G450-AR24 at $M = 1.15$, with respect to structural and aero panel resolutions, the number of modes for flutter analysis, bending stiffness scaling parameter β, and wing sweep angle. The sensitivity analysis results are summarized in Table 2.

Table 2 Sensitivity Analysis Results for Flutter Altitude of ZFW of G450-AR24 at $M = 1.15$.

Number of Wing Aero Panels	Number of Quads in FEM Mesh	Number of Modes Used in Analysis	Bending Stiffness Scaling Parameter β	Sweep Angle (deg)	Flutter Mode ID	Flutter Mach	Flutter Speed (ft/sec)	Dynamic Pressure (psf)	Flutter Altitude (ft)
2083	13014	11	100	0.55	11	1.1506	1240	1349.3	10009
2083	13014	14	100	0.55	11	1.1495	1233	1282.8	11252
2083	13014	11	500	0.55	6	1.1497	1322	2672.7	-8873
2083	13014	14	500	0.55	6	1.1502	1320	2620.8	-8274
2083	13014	18	500	0.55	6	1.1499	1313	2483.6	-6724
3961	13014	14	100	0.55	11	1.1490	1222	1176.1	13411
5907	13014	14	100	0.55	11	1.1510	1229	1227.0	12446
9701	13014	14	100	0.55	11	1.1510	1226	925.9	13108
2083	33384	14	100	0.55	11	1.1493	1245	1423.8	8545
2083	13014	14	100	-10	1	1.1489	1213	1089.0	15328
2083	13014	14	100	-7.6	1 & 11	1.1507	1253	1513.6	6980
2083	13014	14	100	-5	11	1.1489	1240	1371.7	9483
2083	13014	14	100	10	11	1.1501	1282	1928.7	433
2083	13014	14	100	20	6	1.1499	1310	2421.9	-5995

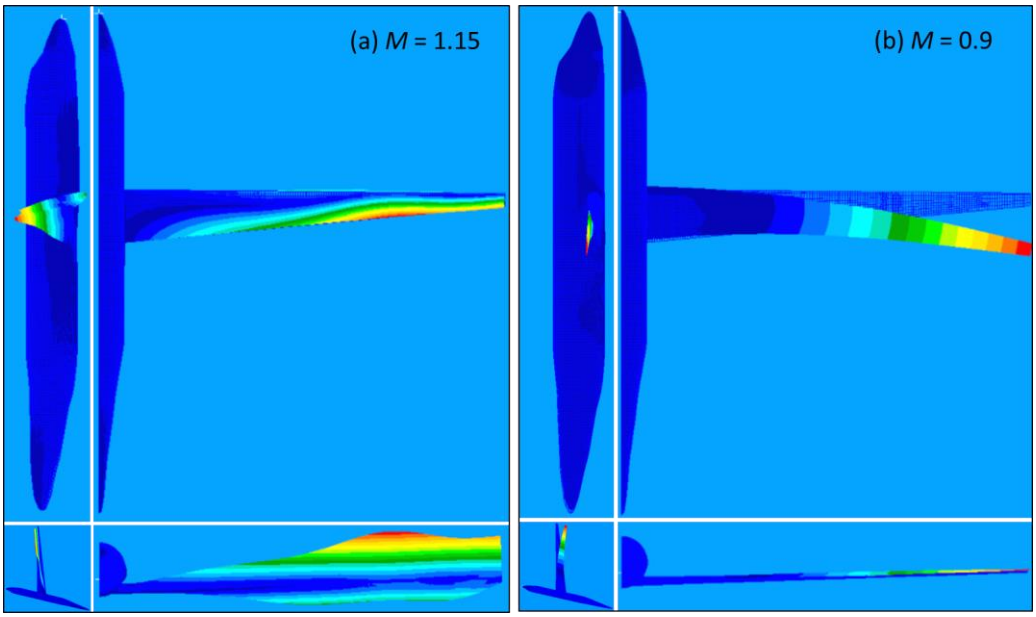

Fig. 7 Flutter mode shapes for ZFW of G450-AR24 at $M = 1.15$ and 0.9.

The wide variation of results in the sensitivity analysis indicates that more study is needed to bring the error margins of flutter altitude prediction within bounds useful for conceptual design. Additional design-of-experiment (DOE) runs with respect to the aero panel aspect ratio and minimum number of aero panels per chord are performed for M = 1.15 and M = 0.9. The flutter mode for M = 1.15 is a complicated wing twist mode (cf. Fig. 7(a)), whereas the flutter mode for M = 0.9 is mainly an in-plane bending mode (cf. Fig. 7(b)). The DOE results in Fig. 8 show that the aero panels have significant influence on the flutter altitude for the wing twist flutter mode, while the flutter altitude for M = 0.9 is almost unchanged for all DOE runs. Further study is required to fully understand how aerodynamic forces affect the flutter characteristics of G450-AR24 at M = 1.15.

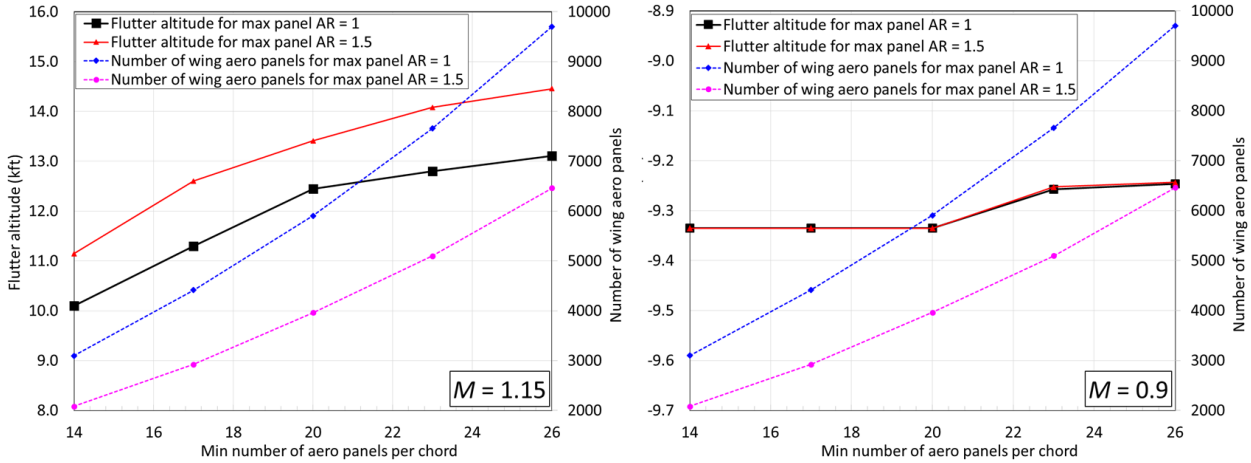

Fig. 8 Flutter altitude sensitivity with respect to aero panels for ZFW of G450-AR24.

The most useful application of flutter analysis during aircraft conceptual design is to gain more insight about an aircraft concept and discover meaningful system-level trades for better flutter margins (such as the flutter altitude sensitivity with respect to β and wing sweep angle). Some general trends in Table 2 are worthy of note. The flutter altitude tends to increase as the number of modes increases; flutter altitude decreases as bending stiffness scaling parameter β increases or wing sweep angle increases; the first wing bending mode becomes more unstable as the wing sweep angle is more negative; eventually, the first wing bending mode becomes a divergent mode once the wing is swept forward enough.

To understand how the bending stiffness scaling parameter affects the flexible modes, the 14th and 15th flexible mode shapes of ZFW of G450-AR24 for β = 500 are shown in Fig. 9. From Figs. 5 and 9, one can see that β has a significant effect on mode shapes. Moreover, for the first 14 flexible modes of ZFW of G450-AR24, the frequency range is from 1.0 Hz to 23.2 Hz when β = 100, while the frequency range is from 1.2 Hz to 26.2 Hz when β = 500. For higher-fidelity flutter analysis, it is necessary to use the equivalent plate theory in Appendix IV and actual stiffened panel constructions to derive the appropriate values of β for various wing and fuselage panels.

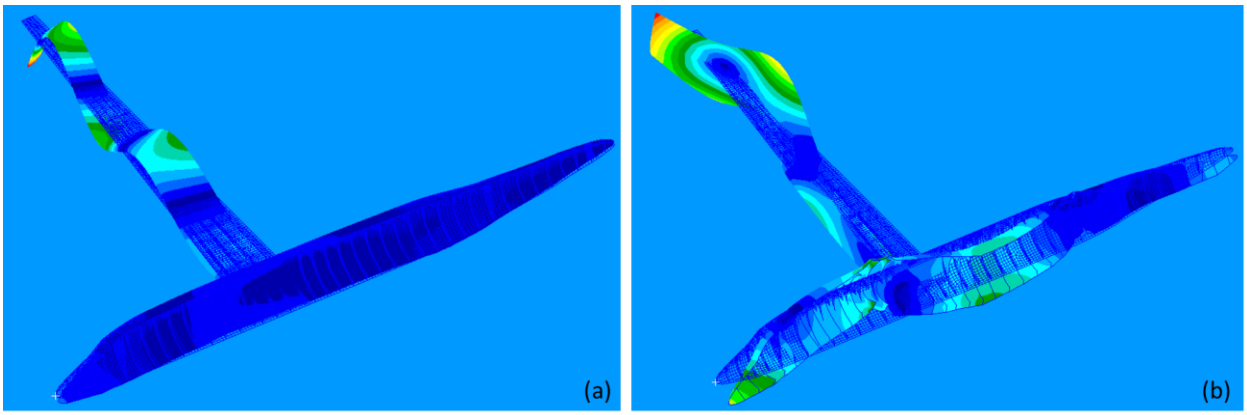

Fig. 9 (a) The 14th and (b) 15th flexible mode shapes for ZFW of G450-AR24 when β = 500.

To better understand the interactions between the wing twist flutter mode and the wing bending divergence mode of ZFW of G450-AR24 at M = 1.15, more sweep angles between -10° and -5° are sampled for flutter analysis. A sweep angle of -7.6° is identified for which the configuration flutters and diverges almost simultaneously at M = 1.15 with a flutter altitude of 6,980 ft. Figure 10 includes the corresponding *V-g*, *V-f*, and root locus plots, while the corresponding divergence and flutter mode shapes are shown in Fig. 11. To see the discontinuous jump in the damping curve before M_V = 0.95 for the divergence mode, the Mach range for the match-point iteration procedure is expanded to the interval [0.92, 1.38] (instead of the default Mach range [0.9·M, 1.1·M] used for match-point flutter solutions). If the wing sweep angle is between -10° and -7.6°, then the divergence mode 1 is dominant, while the flutter mode 11 is dominant when the wing sweep angle is between -7.6° and 10°.

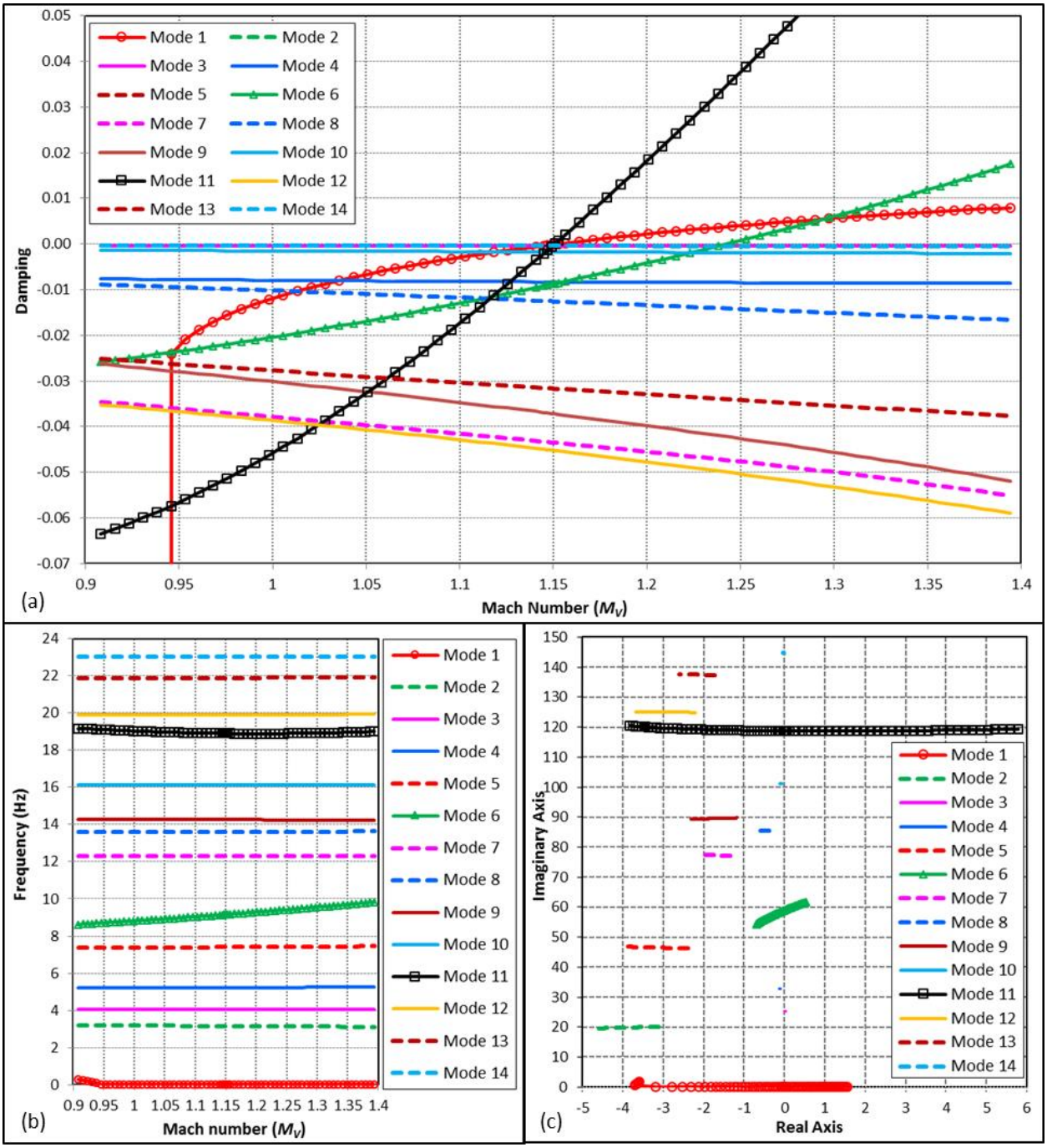

Fig. 10 (a) *V-g*, (b) *V-f*, and (c) root locus plots for ZFW of G450-AR24 (sweep angle = -7.6° and M = 1.15).

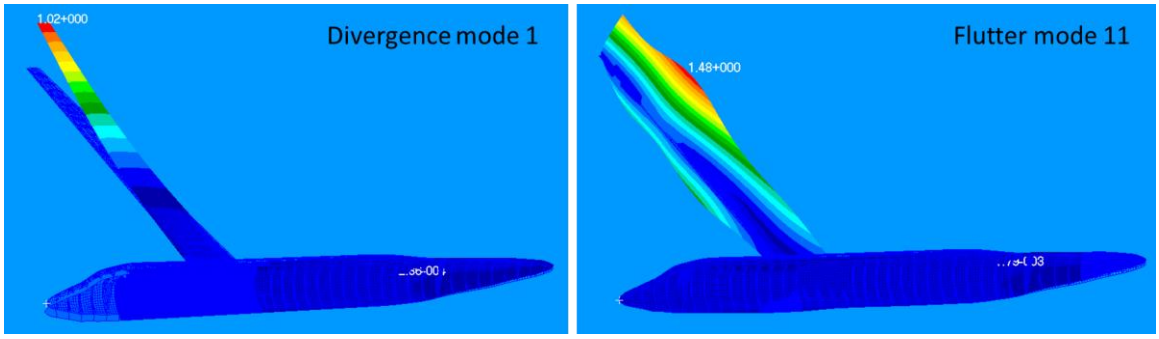

Fig. 11 Divergence and flutter mode shapes for G450-AR24 (sweep angle = -7.6° and M = 1.15).

It is worth noting that a similar flutter mode switch between mode 11 and mode 6 occurs when the sweep angle changes from 10° to 20°. In Fig. 10(a), mode 6 shows an unstable trend around M_V = 1.25, but it is not a flutter mode for M = 1.15 when the sweep angle is -7.6°. As the sweep angle moves from 10° to 20°, mode 6 gradually becomes dominant; when the sweep angle is 20°, mode 6 becomes the flutter mode for M = 1.15 (cf. Table 2).

IV. Concluding Remarks

The proposed match-point iteration procedure finds a flutter boundary point efficiently and robustly. Together with ConceptFEA's rapid structural sizing capability, a conceptual designer can generate flutter boundary curves in (M, Altitude)-plane starting from an OpenVSP geometry model for an aircraft concept within a few days. The flutter analysis results generated by ConceptFEA indicate that the automated flutter analysis process can correctly capture the flutter and divergence physics, at least for a few configurations studied by the authors. ConceptFEA is a conceptual-level analysis tool and there are many conceptual-level uncertainties not quantified in the flutter analysis process. Therefore, the flutter analysis results are more qualitative than quantitative. Further verifications are required to ensure that ConceptFEA is capable of accurately predicting known flutter behaviors of aircraft configurations.

Sensitivity analysis of the predicted flutter altitude of a high aspect-ratio wing configuration is conducted with respect to resolutions of aero and structural panels, the number of modes for flutter analysis, bending stiffness scaling parameter for equivalent panels, and wing sweep angle. All the results are credible qualitatively. Further research is required to understand why aero panel resolution affects the flutter altitude significantly for a wing twist flutter mode of the high aspect-ratio wing configuration.

ConceptFEA has been expanded to provide conceptual designers a tool for rapid flutter assessment starting from an aircraft concept in OpenVSP geometry. Such an analysis capability enables better collaborations between conceptual designers and technology developers. For example, a conceptual designer could get equivalent panels for both membrane and bending actions based on real-world examples of stiffened panels used for aircraft construction. This makes the FEA results for aircraft concepts more credible. For technology assessment, equivalent panels can be based on stiffened panels using new technologies for panel construction and panel materials. Then ConceptFEA analysis helps technology developers and technology investment decision makers understand the system-level impacts of technology research advancements. For technology requirement development, a conceptual designer could find out what kinds of equivalent panels can help achieve certain design goals (such as flutter speed greater than a target value) using ConceptFEA, and use the equivalent plate theory in Appendix IV to determine the requirements for stiffened panels. In all, ConceptFEA fosters more meaningful multidisciplinary interactions.

Appendix I. Method for Selecting Velocities for Damping Curves

Given $V_{min} < V_f < V_{max}$ (in/sec) and an integer $n \geq 10$, generate exactly n velocities $\{V_s: 1 \leq s \leq n\}$ (including V_f) as follows.

1. Find a pair of numbers δ_1 and δ_2 with the following properties:
   (i) $n_1 = (V_f - V_{min})/\delta_1 > 1$ is a positive integer.
   (ii) $n_2 = (V_{max} - V_f)/\delta_2 > 1$ is a positive integer.
   (iii) $n_1 + n_2 = n - 5$.
   (iv) $|\delta_1 - \delta_2|$ has the minimum value among all possible pairs satisfying the previous three conditions.
2. Set $V_s = V_{min} + (s-1)\cdot\delta_1$ for $1 \leq s \leq n_1$.
3. Set $V_s = V_f - \delta_1/2$ for $s = n_1+1$.
4. Set $V_s = V_f - \delta_1/4$ for $s = n_1+2$.

5. Set $V_s = V_f$ for $s = n_1+3$.
6. Set $V_s = V_f + \delta_2/4$ for $s = n_1+4$.
7. Set $V_s = V_f + \delta_2/2$ for $s = n_1+5$.
8. Set $V_s = V_f + (s-n_1-5)\cdot\delta_2$ for $n_1+6 \le s \le n$.

This numerical method generates $\{V_s: 1 \le s \le n\}$ that includes V_f and is as evenly distributed on the interval $[V_{min}, V_{max}]$ as possible with 4 points clustered around V_f. The reason to use n instead of velocity spacing to generate $\{V_s: 1 \le s \le n\}$ is for ease of use. It is much easier to understand how n (instead of velocity spacing) could increase the computational cost or affect the damping curve resolution for flutter analysis. Numerically, increasing n leads to more accurate calculation of the predicted flutter Mach and more evenly distributed velocities.

For V_{min} = 13374 in/sec, V_f = 14859.5 in/sec, V_{max} = 16345.5 in/sec, and n = 20, the above method yields n_1 = 7 and n_2 = 8. The generated velocities $\{V_s: 1 \le s \le n\}$ (all rounded to integers except V_f) = {13374, 13586, 13798, 14011, 14223, 14435, 14647, 14753, 14806, ***14859.5***, 14906, 14952, 15045, 15231, 15417, 15602, 15788, 15974, 16159, 16345}, which includes V_f.

Appendix II. Method for Selecting Reduced Frequencies

Given $k_{min} < k_{max}$, generate a sequence of reduced frequencies $\{k_j\}$ as follows.
1. Set k_1 = 0.001 (the default minimum reduced frequency set by NASTRAN) and j = 2.
2. If $0.005 < k_{min} < 0.04$, set $k_j = k_{min}$ and increase j by 1.
3. Set k_j = 0.05 and increase j by 1.
4. If $0.06 < k_{min} < 0.09$, set k_j = 0.075 and increase j by 1.
5. Set k_j = 0.1 and increase j by 1.
6. If $k_{max} < 1$, set $\delta = k_{max}/10$; otherwise, set δ = 0.1.
7. For the next ten reduced frequencies, set $k_j = k_{j-1} + \delta$ and increase j by 1.
8. Set δ = 0.2 and counter s = 0.
9. While $k_{j-1} < k_{max}$ do the following:
   (i) Set $k_j = k_{j-1} + \delta$ and increase j by 1.
   (ii) Increase s by 1.
   (iii) If s = 6, increase δ by 0.1 and reset s = 0.

The reduced frequencies for all modes involved in flutter analysis are in the interval $[k_{min}, k_{max}]$. The sequence $\{k_j\}$ generated by this numerical method covers the interval $[0.001, k_{max}]$ with a point near k_{min} (if $k_{min} < 0.1$) and the spacing between two consecutive points is gradually increasing. This method aims to attain a good balance between the computational cost (the number of reduced frequencies in $\{k_j\}$) and a reasonable discretization of the reduced frequency interval used in flutter analysis. In Step 9, the spacing between two consecutive k_j's is increased by 0.1 after being used 6 times. One can use a different method to manage the spacing between k_j's. The goal is to avoid generating too many k_j's if k_{max} is relatively large.

If k_{min} = 0.0127 and k_{max} = 1.6274, the above method yields $\{k_j\}$ = {0.001, 0.0127, 0.05, 0.1, 0.2, 0.3, 0.4, 0.5, 0.6, 0.7, 0.8, 0.9, 1.0, 1.1, 1.3, 1.5, 1.7}.

Appendix III. Method for Updating Air Density

For simple cases, Eq. (3) is sufficient for a converged match-point flutter solution in a few iterations. However, if the damping curves have no intersection point with g = 0 (i.e., M_f does not exist), then the challenge is how to update ρ without losing track of where the flutter air density is located. Moreover, Eq. (4) might fail in some cases and Subsection III.B has such an example. The following numerical method for updating air density ensures the termination of the match-point iteration procedure in Section II and guarantees a match-point flutter solution if Eq. (4) holds.

1. Initialization: Set b_l = 0, b_u = 10,000. (This step is only executed once when this method is first used.)
2. Compute the next air density as follows.
   (i) If M_f does not exist, set $\rho_{next} = \rho\cdot(M_{max}/M)^2$.
   (ii) If a damping curve starts with a positive damping coefficient, set $\rho_{next} = \rho\cdot(M_{min}/M)^2$.
   (iii) If it is not any of the two previous cases, set $\rho_{next} = \rho\cdot(M_f/M)^2$.
3. Update the bounds for the flutter air density as follows.
   (i) If $\rho_{next} > \rho$ and $b_l < \rho$, then reset $b_l = \rho$.

(ii) If $\rho_{next} < \rho$ and $b_u > \rho$, then reset $b_u = \rho$.

4. Terminate the match-point iteration procedure if $|b_u - b_l|$ is sufficiently small (e.g., less than 10^{-6}).
5. Modify ρ_{next} as follows to avoid adverse effects of numerical errors.
   (i) If $\rho_{next} < 0.5 \cdot \rho$, then reset $\rho_{next} = 0.5 \cdot \rho$.
   (ii) If $\rho_{next} > 1.5 \cdot \rho$, then reset $\rho_{next} = 1.5 \cdot \rho$.
   (iii) If $\rho_{next} \le b_l$ and $b_u < 10{,}000$, then reset $\rho_{next} = 0.5 \cdot (b_l + b_u)$.
   (iv) If $\rho_{next} \le b_l$ and $b_u = 10{,}000$, then reset $\rho_{next} = 1.05 \cdot b_l$.
   (v) If $\rho_{next} \ge b_u$ and $b_l > 0$, then reset $\rho_{next} = 0.5 \cdot (b_l + b_u)$.
   (vi) If $\rho_{next} \ge b_u$ and $b_l = 0$, then reset $\rho_{next} = 0.95 \cdot b_u$.
6. Replace ρ by ρ_{next}.

The initial upper bound 10,000 can be any sufficiently large number. The monotonicity assumption about M_f given in Eq. (4) might be violated in practice due to numerical analysis errors. So the lower and upper bounds for the flutter air density, as well as the modifications of ρ_{next} in Step 5, make the match-point iteration procedure very robust. The exceptional cases in Step 2 can occur if ρ is far away from the flutter air density.

Appendix IV. Equivalent Plate Theory

For a comprehensive survey of studies conducted since 1914 on the use of equivalent-plate stiffnesses in modeling the overall, stiffness-critical response of stiffened plates and shells, see the paper by Nemeth [21]. The theory in this appendix is only about membrane and bending equivalences of a metallic uniaxial stiffened panel using the same isotropic material for stiffeners and panel. For simplicity, the isotropic material is assumed to have Young's modulus of 1 and Poisson ratio of 0.

Figure 12 shows a cross section of an integral blade stiffened panel, where d_S is the spacing between stiffeners, h_S is the thickness of the equivalent-stiffener layer, and A_S is the area of stiffener cross section.

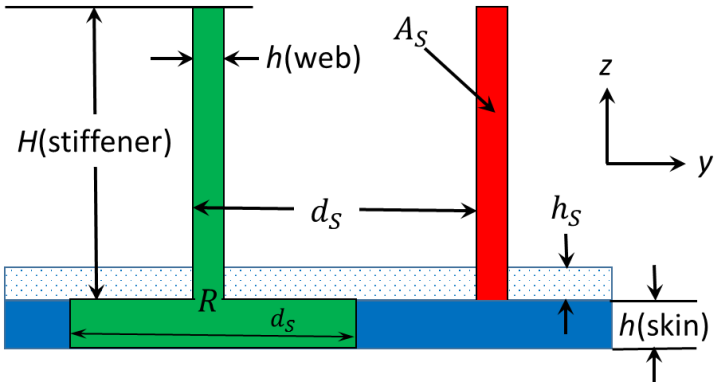

Fig. 12 The cross section dimensions of an integral blade stiffened panel.

Equivalent plate theory aims to replace a stiffened panel by an equivalent [flat] panel with total thickness of (h(skin)+h_S) such that the stiffened and equivalent panels have similar stiffness properties. Four formulas for thickness h_S of equivalent-stiffener layer are given in Ref. [21] and each formula is suitable for certain dominant physical characteristic response involved in finite-element analysis. For equivalence based on membrane action, h_S is defined by the following formula (cf. Eq. (48) in Ref. [21]).

$$h_S = \frac{A_S}{d_S} \tag{5}$$

For an integral blade stiffener in Fig. 12, $A_S = H$(stiffener)$\cdot h$(web). The membrane equivalence can be attained by using (h(skin)+h_S) as the physical thickness of the equivalent panel, but the bending stiffness of the equivalent panel is usually different from the bending stiffness of the stiffened panel.

The NATRAN PSHELL element allows a membrane-equivalent panel to minic the bending stiffness of the stiffened panel. The adjusted bending stiffness D_{11}^* of a membrane-equivalent panel with thickness (h(skin)+h_S) is defined by NASTRAN using a scaling parameter β.

$$D_{11}^{*}(\text{equivalent panel}) = \beta \cdot \frac{(h(\text{skin})+h_S)^3}{12} \tag{6}$$

Therefore, for a proper value of β, the bending stiffness of the membrane-equivalent panel in NASTRAN can be the same as the maximum bending stiffness of the stiffened panel.

Because the material is assumed to have Young's modulus of 1 and Poisson ratio of 0, the maximum bending stiffness D_{yy} of a uniaxial stiffened panel is defined by the following integral.

$$D_{yy} = \frac{1}{d_S} \cdot \iint_R z^2 \, dydz \tag{7}$$

Here R denotes a region consisting of the cross sections of a stiffener and a segment of the base plate with length d_S. For the integral blade stiffened panel in Fig. 12, R is the green region on (y,z)-plane. The location of $z = 0$ defines the reference axis for the bending stiffness. For convenience, the neutral axis of any stiffened or unstiffened panel is used as the reference axis for bending stiffness. Under this assumption, $z = 0$ corresponds to the neutral axis of the stiffened panel. Define the bending stiffness scaling parameter β as follows.

$$\beta = \frac{12 \cdot D_{yy}}{(h_S + h(\text{skin}))^3} \tag{8}$$

Then a membrane-equivalent panel in NASTRAN with its bending stiffness scaling parameter β defined by Eq. (8) has similar properties as the stiffened panel with respect to membrane and bending actions.

The uniaxial stiffened panel analysis tool in HyperSizer [22] can be used to calculate β and verify the equivalences. For any uniaxial stiffened panel, construct the stiffened panel in HyperSizer with an isotropic material that has Young's modulus of 1 and poisson ratio close to zero. The material can be arbitrarily defined with (stiffness for tension) = (stiffness for compression) ≈ 2·(stiffness for in-plane shear). Then the off-diagonal entries in the membrane and bending stiffness matrices are close to zero. Next, construct the equivalent panel with (h(skin)+h_S) as the physical thickness. Rerun the component analysis for the equivalent panel. Then the following equalities must hold.

$$A_{11}(\text{stiffened panel}) = A_{11}(\text{equivalent panel}) = h(\text{skin}) + h_S \tag{9}$$

Here A_{11} is the 1st diagonal entry of the membrane stiffness matrix generated by HyperSizer. Moreover, the bending stiffness entry D_{11}(stiffened panel) generated by HyperSizer with respect to neutral axis (which is labeled as the symmetric D_{11} in HyperSizer) is D_{yy} and

$$\beta = \frac{12 \cdot D_{yy}}{(h(\text{skin})+h_S)^3} = \frac{12 \cdot D_{11}(\text{stiffened panel})}{(A_{11})^3} = \frac{D_{11}(\text{stiffened panel})}{D_{11}(\text{equivalent panel})} \tag{10}$$

So β defined by Eq. (8) does scale the bending stiffness of the membrane-equivalent panel to the maximum bending stiffness of the stiffened panel.

An integral blade stiffened panel example is given on page 653 of Ref. [23]. In this example, h(skin) = 0.049 in, h(web) = 0.153 in, H(stiffener) = 1.026 in, and d_S = 2.194 in. The HyperSizer component analysis yields h(skin)+h_S = A_{11} = 0.12055, h_S = 0.0715, and $\beta = 12 \cdot D_{11}(\text{stiffened panel})/(A_{11})^3$ = 100.6. Of course, one could also compute A_S and D_{yy} manually; then, use Eqs. (5), (7), and (8) to get the same h_S and β.

Acknowledgments

This work is funded by the NASA Commercial Supersonic Technology Project and the NASA Transformational Tools & Technologies Project. The authors would like to thank James Fenbert for technical discussions that significantly improved the paper.

References

[1] Hassig, H., "An Approximate True Damping Solution of the Flutter Equation by Determinant Iteration," *Journal of Aircraft*, Vol. 8, No. 11, 1971, pp. 885-889.

[2] Rodden, W., Harder, R., and Bellinger, E., "Aeroelastic Addition to NASTRAN," NASA CR-3094, 1979.

[3] NASTRAN, "Aeroelastic Analysis User's Guide," MSC Software Corporation, 2018.

[4] ZAERO, "Application's Manual Vol. 1 – Engineers' Toolkit for Aeroelastic Solutions," ZONA Technology Inc., Scottsdale, AZ, June 2011.

[5] Lind, R., and Brenner, M., "Robust Flutter Margins of an F/A-18 Aircraft from Aeroelastic Flight Data," *Journal of Guidance, Control, and Dynamics*, Vol. 20, No. 3, 1997, pp. 597-604.
[6] Pitt, D., "A New Non-Iterative P-K Match Point Flutter Solution," AIAA Paper 1999-1353, April 1999.
[7] Britt, R., Jacobson, S., and Arthurs, T., "Aeroservoelastic Analysis of the B-2 Bomber," *Journal of Aircraft*, Vol. 37, No. 5, 2000, pp. 745-752.
[8] Lind, R., "Flight-Test Evaluation of Flutter Prediction Methods," *Journal of Aircraft*, Vol. 40, No. 5, 2003, pp. 964-970.
[9] Goodman, C., Hood, M., Reichenbach, E., and Yurkovich, R., "An Analysis of the F/A-18C/D Limit Cycle Oscillation Solution," AIAA Paper 2003-1424, April 2003.
[10] Silva, W., Garza, A., Zink, S., Bounajem, E., Johnson, J., Buonanno, M., Sanetrik, M., Chwalowski, P., Yoo, S., and Hur, J., "An Overview of the NASA High Speed ASE Project: Aeroelastic Analyses of a Low-Boom Supersonic Configuration," AIAA Paper 2015-0684, January 2015.
[11] Li, W., Geiselhart, K., Olson, E., and Robinson, J., "Automation of Structural Sizing of Aircraft Concepts Under Static Aeroelastic Constraints," AIAA Paper 2018-0103, January 2018.
[12] Mccullers, L., "FLOPS User Guide," NASA Langley Research Center, Hampton, Virginia, 2008.
[13] OpenVSP, Version 3.11.0, Open Source, URL:http://www.openvsp.org [retrieved 9 July 2018].
[14] NASTRAN, Version 2016.0, MSC Software, URL:http://www.mscsoftware.com/product/msc-nastran [retrieved 9 July 2018].
[15] PATRAN, Version 2012.2 64-Bit, MSC Software, URL:http://www.mscsoftware.com/product/patran [retrieved 9 July 2018].
[16] Li, W., and Robinson, J., "Automated Generation of Finite-Element Meshes for Aircraft Conceptual Design," AIAA Paper 2016-3287, June 2016.
[17] FAR Part 25, "Airworthiness Standards: Transport Category Airplanes," Federal Aviation Administration, US Department of Transportation, URL:https://www.gpo.gov/fdsys/pkg/CFR-2013-title14-vol1/pdf/CFR-2013-title14-vol1-part25.pdf [retrieved 9 July 2018].
[18] Gulfstream G450, "G450 Specifications," Gulfstream Aerospace Corporation, 2015. URL:http://www.gulfstream.com/images/uploads/brochures/aircraft/G450SpecSheet.pdf [retrieved 9 July 2018].
[19] Sensmeier, M., and Samareh, J., "A Study of Vehicle Structural Layouts in Post-WWII Aircraft," AIAA Paper 2004-1624, April 2004.
[20] Code7700, "Limitations: Gulfstream G450," URL:http://code7700.com/g450_limitations.htm [retrieved 9 July 2018].
[21] Nemeth, M., "Treatise on Equivalent-Plate Stiffnesses for Stiffened Laminated-Composite Plates and Plate-Like Lattices," NASA TP-2011-216882, 2011.
[22] HyperSizer, Version 7.1.43, Collier Research and Development Inc., URL:http://hypersizer.com [retrieved 9 July 2018].
[23] Niu, M., *Airframe Stress Analysis and Sizing, 2nd Edition*, Conmilit Press, Ltd., Hong Kong, 2001.